

A&A manuscript no.
(will be inserted by hand later)

Your thesaurus codes are:
11 (11.06.2; 11.07.1; 11.11.1; 11.19.6)

ASTRONOMY
AND
ASTROPHYSICS
2.12.2024

Multi-component models for disk galaxies

I. Stellar rotation and anisotropy

Ezio Pignatelli and Giuseppe Galletta

Dipartimento di Astronomia, Università di Padova,
Vicolo dell' Osservatorio, 5, I-35122 Padova, Italy.

Received; accepted

Abstract. We present here a self-consistent, tridimensional model of disc galaxy composed by ellipsoidal distributions of matter with different flattening and density profiles. The particular case of disc galaxies composed by two spheroidal bodies (disc + bulge) has been studied, deriving the detailed stellar kinematics in every point of the galaxy projected on the sky plane. We adopted two components: an exponential disc and a bulge following the $r^{1/4}$ law.

To produce a library of rotation- and velocity dispersion- profiles directly comparable with observations of stellar kinematics, a set of model has been used simulating the sequence of S0s and Spirals, identified by an increasing disc-to-bulge ratio. Inside every class, kinematical curves were produced by changing the relative concentration of the two components and the inclination of the galaxy with respect to the line of sight. Such curves can be directly compared with observations of stellar kinematic by means of two scaling factors: the total mass of the galaxy, and the effective radius.

The model allows also to detect the presence of anisotropy in the velocity distribution. In the special case of S0s, we explored the sensitivity of the model kinematical curves to changes in the anisotropy and flattening of the bulge. Our method uses the comparison between the stellar rotation curve, measured along the major axis, and another curve taken with an offset parallel to the major axis. For intermediate ($0.4 \leq b/a \leq 0.85$) flattenings, even with an error of 40-50% in the maximum rotational velocity measured, it is possible to distinguish a change of anisotropy of 15%.

Key words: Galaxies: fundamental parameters – Galaxies: general – Galaxies: kinematics and dynamics – Galaxies: structure

1. Introduction.

The study of the stellar distribution and kinematics in disk galaxies is an important tool to understand their structure. It is the only way to study stellar systems with are gas poor, such as S0s, and it is crucial to distinguish between different scenarios of galaxy formation. It allows to discuss if a bulge is flattened by rotation or by anisotropic residual velocities and how the different components of a galaxy mutually interact.

In the past, in front of the success achieved in studying the *gas* kinematics of disk galaxies, much less attention has been paid to the modeling of their *stellar* kinematics from the observations. A reason of this was the lower extension of the available stellar rotation curves, based on absorption lines, with respect to that obtained with emission lines (optical or 21cm). However, the inner part of the galaxies is often poor of cold gas, and can be studied with data from the stellar component only. In addition, the progresses in detectors and data analysis techniques (Sargent et al. 1977, Bertola et al. 1984, Kuijken & Merrifield 1993) extended the range explored with stellar data and produced a large quantity of stellar rotation- and velocity dispersion- curves, making compulsory the creation of realistic theoretical models for their interpretation.

Send offprint requests to: G. Galletta

However, the modeling of stellar components in disk galaxies must overcome several difficulties. First, the non-negligible thickness of stellar disks, compared to the gas ones, that requires a tridimensional approach. Second, the fact that the observed rotation curve does not represent the circular rotation defined by the potential, because of the partial transparency of the stellar body and of the presence of the velocity dispersion. The stellar rotation curves are integrated along the line-of-sight across regions of different kinematics and are influenced by the gradient of mass of these regions. The influence of the velocity dispersion and its eventual anisotropy are particularly important in early-type galaxies, where the velocity dispersion is of the same order of magnitude of the rotational velocity.

The last effect is known with the name of *asymmetric drift* and the first attempt to evaluate it from observations date back to 1961, with the van der Hulst's work on the observations of NGC 4111 made by Humason and Oort (Van der Hulst 1961). More recently, the influence of the asymmetric drift on the stellar rotation curves has been taken into account by some authors (Bertola & Capaccioli 1975, Kormendy 1984, Illingworth & Schechter 1982, Fillmore et al. 1986, Zeilinger et al. 1990). These theoretical models and interpretations of stellar kinematics were assuming an isotropic velocity dispersion or were limited to edge-on galaxies. Most part of models were simulating the galaxy by means of the disk component only, with the only exceptions of the Fillmore et al. (1986) model and the Zeilinger et al. (1990) work. Both papers were based on non self-consistent models and the first one made use of photometrical data only.

An improvement of the understanding of the stellar systems may be obtained with a tridimensional, self-consistent model of galaxy made of different components whose parameters are constrained by the observed photometry and stellar kinematics. It must take into account the effects of the integration of these data projected along the line of sight as well as that of the asymmetric drift.

We present here a self-consistent, multi-component model of disk galaxy based on an analytic approach to the problem. We also try to derive the relations between the observed properties and the model parameters that can be useful to observers in interpreting the data of a single galaxy.

2. The hypothesis of the model

2.1. The density profiles

We want to describe a stellar system as much similar to a real one, and in particular to a disk galaxy. A first step is to define a suitable distribution function $f(x, v)$ containing the tridimensional structure of the galaxy and its velocity field.

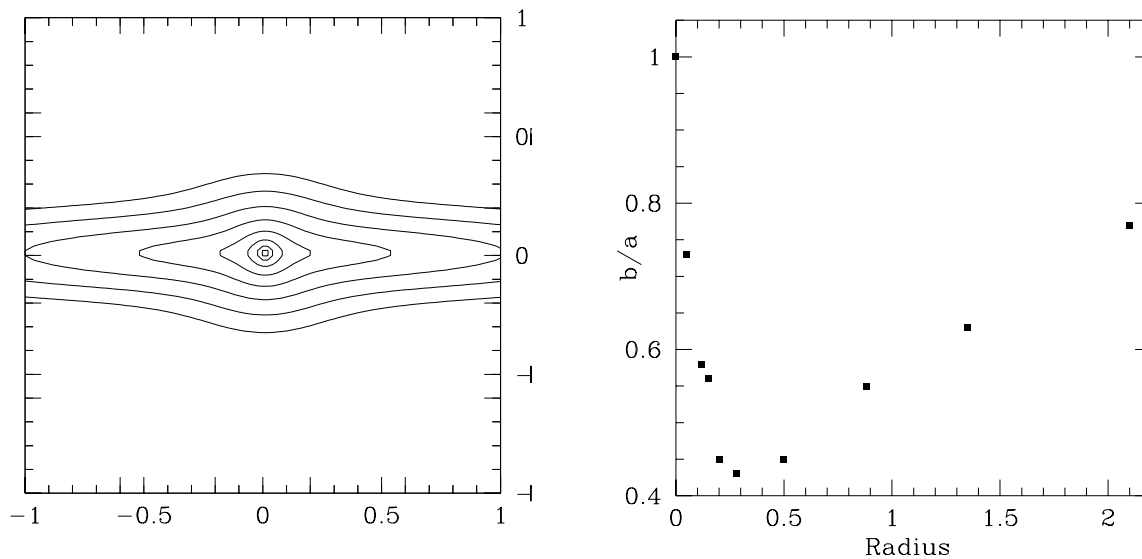


Fig. 1. **Left:** Isophotes of a model composed by a spherical bulge following the $R^{1/4}$ law, and an exponential disc with $b/a = 0.1$. **Right:** The global axial ratio of the model shown in 1 as function of the radius. Note the peak of isophote flattening at intermediate radii, obtained with two components of constant flattening.

The structure of the disk galaxies can be modeled by the mixing of different components: a bulge, a disk and eventually a halo. Every single component may be reproduced by an ellipsoidal density distribution whose projection on the sky generates elliptical shapes. If the axial ratio of each one of these components is constant with radius, but different for every component, we can apply a generalization of the Newton's theorems for spherical bodies, that makes simpler the calculation of the kinematical properties. This approximation allows anyhow to generate projected light distributions with variable ellipticity, as observed. This is due to the predominance of the different components at different distances from the nucleus. An example of a composite light distribution - which is rounder in the center and in the outer regions, while flattens at intermediate radii - is given in Fig. 1. Spindle isophotes may also be reproduced in this way.

Another choice concerns the shape of the different components. Differently from the studies on the elliptical galaxies, the works made on the shape of the disks reveals slightly or absent deviations from the oblateness (Sandage et al. 1970, Grosbøl 1985, Binney & de Vaucouleurs 1981, Magrelli et al. 1992). The mean deviation suggested should be $\leq 5\%$. A different situation is found in some bulges, whose structure may range from slight triaxial (Bertola et al. 1991) to strongly triaxial in rare cases (Stark 1977). Taking into account these facts, we decided to assume a cylindrical symmetry for the galaxy's components. This seems to be a good compromise between a "realistic" description of a single galaxy, yet with a large number of free parameters, and a general deduction of the galaxy dynamics and structure with the minimum number of constraint obtained from the observations.

Given the previous hypotheses, the density profile of each component can be described in terms of the radial coordinate only, with the values of their parameters constrained by observations.

As shown by Young (1976), the $r^{1/4}$ luminosity profile followed by the elliptical galaxies and the bulges can be deprojected obtaining an intrinsic density law. This latter can be approximated by the analytical formula:

$$\rho_B(r) = \rho_{0B} \frac{e^{-bx^{1/4}}}{x^{7/8}} \quad (1)$$

where $x=r/R_{eB}$ and $b = 7.66924944$, which is valid for every ellipticity value of the galaxy. R_{eB} is the bulge effective radius, corresponding to the distance from center in which half of the total bulge luminosity is contained.

For the disk component, the observed exponential profile can be deprojected generating the law:

$$\rho(r) = \rho_{0D} \alpha K_0(\alpha r) \quad (2)$$

where K_0 is the incomplete Bessel function of order zero, and $1/\alpha$ is the disk scale length. The disk effective radius is $R_{eD}=1.6784/\alpha$.

The above laws may be cut at a radius R_{max} for computation purposes, and put together to produce a very wide range of complex global density distributions. The introduction of an (usually dark) halo among the galaxy components is needed when kinematics at large galactocentric radii are considered. In this paper, we shall explore structures composed by two bright components only, omitting the introduction of a dark halo. This choice follows the fact that in the most part of stellar rotation curves presented in the literature the regions explored are limited to the luminous component inside $1 - 2R_e$.

2.2. The velocity distribution

When the spatial dependence of the distribution function $f(x, v)$ is determined by the combination of the above density laws, the velocity distribution can be obtained by integrating the collisionless Boltzmann equation producing the moments equations. This will make the galaxy model self-consistent, warranting its dynamical equilibrium, such as in real systems.

In order to close the system of the moment equations, some additional assumptions are needed on the model. This may be obtained by imposing some restrictions on the shape of the velocity ellipsoid.

We assume the following constraints:

- The ellipsoid's principal axes remain aligned with the cylindric coordinate system (R, ϕ, z) , so that $\sigma_{Rz} = \sigma_{R\phi} = \sigma_{\phi z} = 0$; this assumption describes a situation similar to that of the solar neighborhood, where the deviation of the velocity ellipsoids from the cylindric coordinate axes is low.
- The ratios of the components of the tensor σ_{ij}^2 are constant inside the galaxy, so that we can write

$$\sigma^2 = s(\mathbf{x})\sigma(0) \quad (3)$$

where $s(\mathbf{x})$ is a scalar function of the coordinates. The choice produces velocity ellipsoids with same shape in every point of the galaxy. This may be an arbitrary assumption, but is more general than the usual hypothesis of isotropy of the velocity ellipsoids ($\sigma_{RR} = \sigma_{\phi\phi} = \sigma_{zz}$).

– A final requirement is the adoption of: $\sigma_{\phi\phi} = \sigma_{RR}$, in every region of the galaxy. We preferred this assumption to the widely used $\sigma_{RR} = \sigma_{zz}$ because our assumption is the simplest possible with a distribution function involving a third integral $f(E, L_z, I_3)$. The other hypothesis implicitly describe a system with two integrals of motion or $f(E, L_z)$ (Binney et al. 1990).

Under these limits, needed to simplify the equations and to reduce the number of free parameters, we can describe the velocity dispersion field by means of $\sigma_{RR}(R, z)$ and the homogeneous *anisotropy parameter* β , where

$$\beta \equiv 1 - \frac{\sigma_{zz}^2}{\sigma_{RR}^2} \quad (4)$$

3. The equations

A second step is to derive the main galaxy parameters to be directly compared with the observed mean velocity- and velocity dispersion- curves and with the observed luminosity profile. This latter is coincident with the projected density profile when galaxies are gas-poor and no relevant halo is present.

Independently from the chosen density distribution, the Jeans equations in cylindrical coordinates for a steady-state, axisymmetric system having a velocity ellipsoid described by the above equations produce:

$$\sigma_{RR}^2(R, z) = \frac{1}{\rho(1-\beta)} \int_z^\infty \rho \frac{\partial \Phi}{\partial z} dz \quad (5)$$

$$V_{\text{rot}}^2(R, z) = \sigma_{RR}^2 \frac{\partial \ln \rho \sigma_{RR}^2(R, z)}{\partial \ln R} + \beta \sigma_{RR}^2(R, z) + \rho \frac{\partial \Phi}{\partial R} \quad (6)$$

The partial derivatives of the potential in these equations can be calculated by making use of the relations for a single elliptical component and of the additive property of the potential:

$$\frac{\partial \Phi}{\partial R} = \sum_i 2\pi G R \sqrt{1 - e_i^2} \int_0^\infty \frac{\rho_i(m^2)}{(\tau + 1)^2 \sqrt{\tau + 1 - e_i^2}} d\tau \quad (7)$$

$$\frac{\partial \Phi}{\partial z} = \sum_i 2\pi G z \sqrt{1 - e_i^2} \int_0^\infty \frac{\rho_i(m^2)}{(\tau + 1)(\tau + 1 - e_i^2)^{3/2}} d\tau \quad (8)$$

We defined, following the notation of Binney & Tremaine (1987),

$$m^2 \equiv \frac{R^2}{1 + \tau} + \frac{z^2}{\tau + 1 - e^2} \quad (9)$$

where $e = \sqrt{1 - b/a}$ is the ellipticity of the component.

As a final step, the (ρ, V, σ) quantities must be integrated along the line of sight to produce the observables to be compared with the data. This is done by making use of the general formula:

$$\langle Q \rangle (R_{\text{proj}}, z) = \frac{2 \int_{R_{\text{proj}}}^{\sqrt{R_{\text{max}}^2 - z^2}} \rho(R, z) Q(R, z) R dR}{2 \int_{R_{\text{proj}}}^{\sqrt{R_{\text{max}}^2 - z^2}} \rho(R, z) R dR}$$

where the notation $\langle Q \rangle (R_{\text{proj}}, z)$ is used to indicate the generic quantity Q integrated along the line of sight at the position (R_{proj}, z) on the plane of the sky. Note that we do not restrict our investigation to the case of major-or minor axis profiles.

The luminosity profile was derived analytically in the spherical case for the density profiles given above; the general case where a galaxy with intrinsic flattening p is observed at apparent flattening $\hat{p}^2 = p^2 \sin^2 i + \cos^2 i$ is obtained by making use of the superposition principle and of the general law, derived in Appendix A.2:

$$I(b)_{\text{spheroidal}} = \frac{p}{\hat{p}} I \left(\frac{b}{\hat{p}} \sqrt{\hat{p}^2 \cos^2 \Phi + \sin^2 \Phi} \right)_{\text{spherical}} \quad (10)$$

The component of the velocity dispersion in the direction of the line of sight can be expressed as $\sigma_{\text{obs}}^2 = \sigma^2 (1 - \beta^2 \cos^2 i)$ where i is the angle of inclination of the galaxy ($i = 90^\circ$ corresponds to an edge-on galaxy).

The rotation velocity along the line of sight is $V_{\text{obs}} = V \sin i \cos \phi$, where ϕ is the azimuthal coordinate.

4. The parameters

The model described in the previous sections is so determined by 8 free parameters: the ellipticities e_B , e_D of the bulge and disk component, their total mass and scale length M_D , M_B , R_{eB} , R_{eD} , the ratio of their (M/L) values and the β above defined.

Two of these parameters can be considered scale factors respectively for the mass (and so, the kinematical quantities) and the lengths. We want to choose these scale factors in a way that makes simpler the comparison with the observations, so we select the *global* mass M_{tot} of the model and the *global* R_e (defined as the major axis isophotal radius inside which lies half of the total luminosity) as the scale factors.

The models are then presented in an adimensional form, with six (adimensional) parameters: the two axial ratios, the ratios $\eta = M_B/M_D$ and $\xi = R_{eB}/R_{eD}$, β and the ratio of the (M/L) values. The parameter η represents the ‘physical’ bulge-to-disk ratio and the ξ the concentration of the bulge with respect to the disk.

While the relation between η , M_B , M_D and M_{tot} is obvious, the relation between ξ , R_{eB} , R_{eD} and R_e is more complex. In general, R_e can be evaluated by solving numerically the equation:

$$\frac{(1-\eta)}{2} - (1 + 1.6484x)e^{-1.6484x} + \eta P \left[8, b \left(\frac{x}{\xi} \right) \right] = 0 \quad (11)$$

where $x \equiv R_e/R_{eD}$. In the two extreme cases of pure bulge and pure disk models, we obtain $x = \xi$ or $x = 1$ respectively. Since usually one put $R_{eB} < R_{eD}$, we get $x \in [0, 1]$. In Tab. 1 we show some reference value for models with different values of (ξ, η) .

Table 1. Different values of $x \equiv R_e/R_{eD}$ for different values of the (η, ξ) parameters as discussed in Eq. (11). The different values of η correspond, according to Simien and de Vaucouleurs (1986) to different Hubble types ranging from S0 to Sd.

Hubble Type	η	ξ								
		0.1	0.2	0.3	0.4	0.5	0.6	0.7	0.8	0.9
S0	1.50	0.28	0.45	0.56	0.65	0.73	0.79	0.85	0.91	0.95
Sa	0.68	0.54	0.63	0.72	0.78	0.83	0.87	0.91	0.94	0.97
Sab	0.50	0.64	0.71	0.77	0.82	0.86	0.90	0.93	0.95	0.98
Sb	0.31	0.76	0.80	0.84	0.88	0.91	0.93	0.95	0.97	0.99
Sbc	0.20	0.84	0.87	0.89	0.92	0.94	0.95	0.97	0.98	0.99
Sc	0.10	0.91	0.93	0.94	0.96	0.97	0.97	0.98	0.99	1.00
Scd	0.04	0.96	0.97	0.97	0.98	0.99	0.99	0.99	1.00	1.00
Sd	0.01	0.99	0.99	0.99	0.99	0.99	1.00	1.00	1.00	1.00

We didn’t fully cover the allowed space of these parameters, since some of them are never observed in galaxies: in particular, we kept fixed a $(b/a)_D = 0.1$ value, which seems a reasonable value for the observed disks, and we forced, in first approximation, the M/L ratio of the bulge component to be twice the corresponding disk value. This assumption could be corrected during the fit with observed values (see §5.1).

We do expect that the four remaining free parameters will cover two different physical characteristics: the couple (η, ξ) will somehow reproduce the morphological behavior of galaxies along the Hubble diagram, while the couple (e_B, β) will give us informations about the dynamic of the bulge (rotation- or pressure- supported) of the galaxy.

In the next section we will discuss how these parameters could affect the projected kinematical profiles.

5. The results

The model offers several possible applications of the stellar component of disc galaxies to the observed data. We choose here to illustrate two general applications, starting from observed kinematical data. They are the deduction of the mass ratio between the disk and the bulge and the possibility to detect the presence of anisotropies in the velocity dispersion field.

5.1. The models and the Hubble diagram

The classification of galaxies in a single unificating scheme has been one of the earlier results in the study of stellar systems. The details of this classification are, however, still under discussion. Along the sequence of disk galaxies, the

classification of galaxies may be expressed in terms of photometric properties, such as the relative weights of the bulge and disk component and their relative concentration. Our model allow a dynamical deduction of these properties. We can compare observed velocity- and velocity dispersion- curves with that of a model galaxy, projected at the same viewing angle of the real galaxy and integrated along the line-of-sight. In such a way, one can deduce the disk-to-bulge ratio of the galaxy in terms of mass ratio and relative concentration of the two components. We expect that this dynamical description may give different results with respect to the disk/bulge ratio photometrically deduced. In such a way, it will be possible to correct the M/L ratio assumed and eventually detect the presence of dark matter contained in the inner/intermediate portion of the galaxy.

To make this comparison easy, the adimensional quantities V_{mod} , σ_{mod} , produced by the model should be correlated the physical parameters. Since the model quantities are produced in the adimensional system having $GM_{\text{tot}} = 1$ and $R_{\text{etot}} = 1$, they can be related to the observables by the use of the simple scaling law:

$$V_{\text{obs}} = \sqrt{\frac{GM_{\text{tot}}}{R_{\text{etot}}}} \cdot V_{\text{mod}}$$

$$\sigma_{\text{obs}} = \sqrt{\frac{GM_{\text{tot}}}{R_{\text{etot}}}} \cdot \sigma_{\text{mod}}$$

We then produced a set of rotation- and velocity dispersion curves for six type of galaxies having different bulge-to-disk mass ratio (η) and concentrations (ξ), and with a given $M_{\text{tot}} = 10^{11} M_{\odot}$, and $R_{\text{etot}} = 10 \text{ kpc}$. In this simulation, the model galaxies have an isotropic velocity dispersion. We shall show in the next paragraph how an anisotropic velocity dispersion influence the observed curves.

The curves are presented with the galaxy seen edge-on (90°) and at an inclination of 60° and 30° (Figs. 2–9). They are arranged in terms of η with the curves having different ξ shown in the same panel. The choice of the η values has been made trying to reproduce the main Hubble stages, from S0 to Sd, in agreement with the values deduced by Simien & de Vaucouleurs (1986) listed in Tab. 1. The relation between the observed curves with that presented in the figures is then:

$$V_{\text{obs}} = \sqrt{\frac{M_{\text{tot}}/[10^{11} M_{\odot}]}{R_{\text{etot}}/[10 \text{ kpc}]}} \cdot V_{\text{fig}}$$

$$\sigma_{\text{obs}} = \sqrt{\frac{M_{\text{tot}}/[10^{11} M_{\odot}]}{R_{\text{etot}}/[10 \text{ kpc}]}} \cdot \sigma_{\text{fig}}$$

with masses computed in solar mass units and radii in Kpc.

This procedure allows, within some limits, to consider the galaxy as a unique structure, with a typical bulge/disk ratio and bulge concentration. However, it fits also into the idea that it is possible to distinguish dynamically the galaxy type. This approach has been faced by Persic and Salucci (1995) on the basis of a sample of galaxies taken from the literature. Working on the superposition of nearly 1000 observed gas rotation curves grouped for Hubble type, the authors derived a circular rotation curve for every given Hubble type. However, since this work was mainly aimed to the detection of dark matter, more care is devoted to the outer part of the rotation curves; in addition, a poor statistic is available on the early-type disk galaxies S0 and Sa.

5.2. The anisotropy in bulges

The low rotational velocities found in elliptical galaxies with respect to their flattening (Bertola & Capaccioli 1977, Kormendy & Illingworth 1977) can be interpreted in terms of anisotropy in the stellar velocity distribution (Binney 1978). The same indications arose from the study of the velocity dispersion profiles (Tonry 1983). For similarity with elliptical galaxies, we can expect that some anisotropy could be present in bulge dynamics also. On the contrary, the presence of anisotropy in the disk component of the galaxies should be less relevant, due to the lower value of the velocity dispersion of disks compared with bulges or elliptical galaxies.

The study of velocity anisotropy in disk galaxies may give indications on the differences existing between bulges and ellipticals, contributing to understand the formation process of this two classes of objects. However, due to the composite nature of disk galaxies, to measure the anisotropy of the velocity distribution from the observables (V, σ) is much more difficult than in the case of elliptical galaxies. Working on the same set of data, concerning four S0 and Sa galaxies, Kormendy & Illingworth (1982) claim the isotropy of their bulges, while Whitmore, Rubin and Ford (1985) deduce the opposite conclusion. Both authors used the V/σ test, first proposed by Binney (1976) for Elliptical

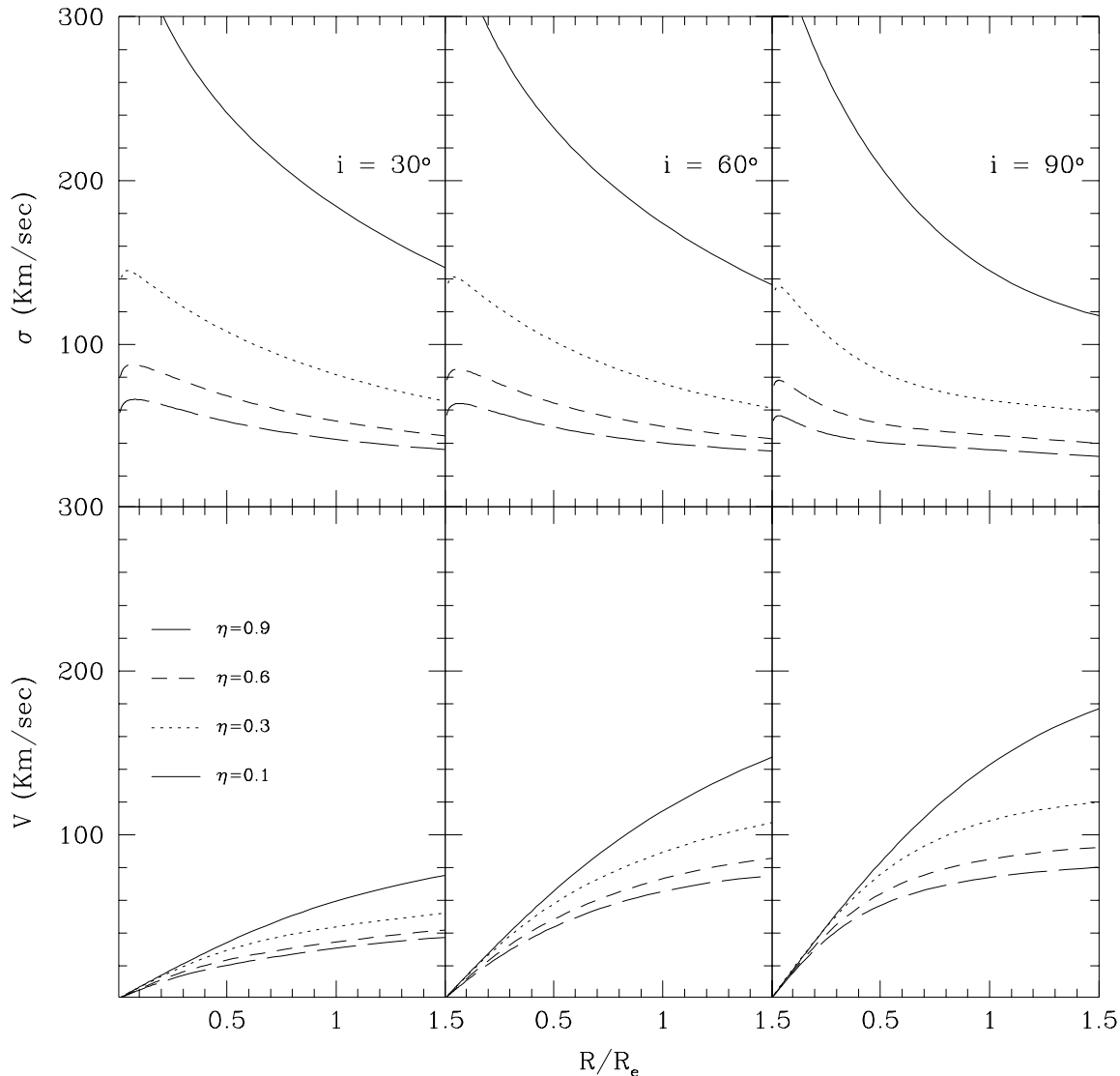


Fig. 2. Rotation curved and velocity dispersion profiles for S0 galaxies, varying the concentration of the bulge relative to the disk components, and the inclination angle i . All the quantities are referred to a galaxy of $M = 10^{11}M_{\odot}$, and $R_e = 10$ kpc. The scaling factor is described into the text.

galaxies. The fact that the same data may be interpreted in such different ways clearly demonstrates the ambiguity of this test, when applied to the bulges of disk galaxies.

In a model of galaxy, the shape of the potential defines, on the galaxy plane, the shape of the rotation- and velocity dispersion- profiles. However, the ratio of the central velocity dispersion to the maximum rotational velocity is dependent both from the ellipticity e and from the anisotropy parameter β : one may obtain in a model a higher V/σ ratio increasing the ellipticity and/or decreasing the anisotropy parameter. As a reverse argument, we can deduce the galaxy potential by fitting the observed rotation curve along the apparent major axis but we cannot deduce from this curve the values of e or β . To define the values of these parameters, we need more observable constraints.

One of this may arise from the photometry; in particular, from the ellipticity value obtained by fitting the observed isophotes. In such a case, the β parameter can be, in principle, derived from the major axis kinematical curves (V and σ) only. Such a case is however so rarely found in the literature, due to the great errors that can derive from

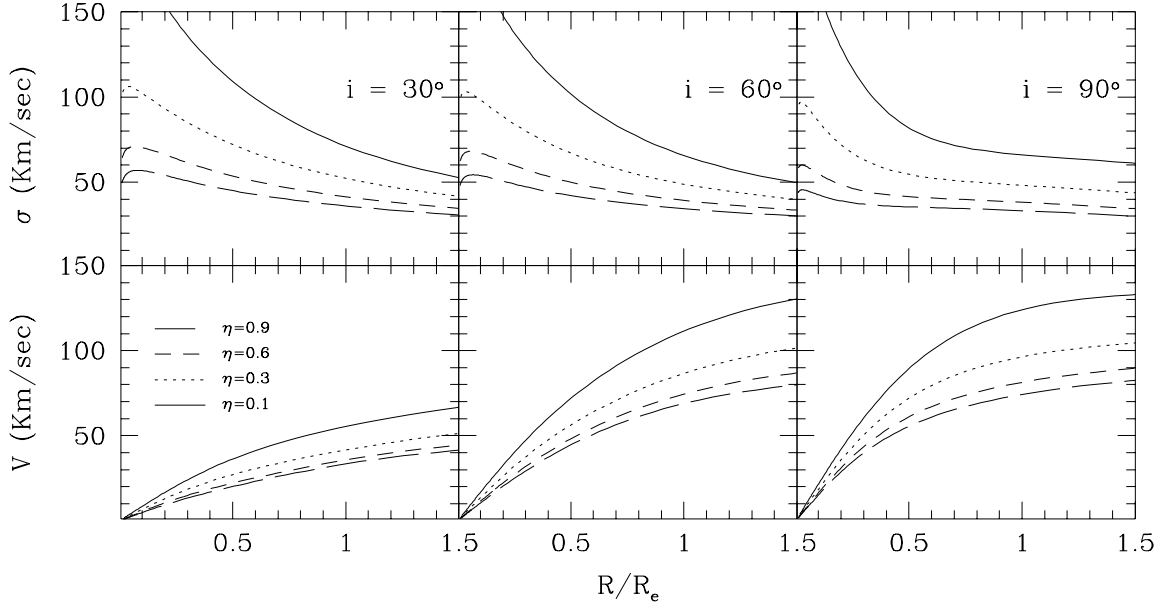


Fig. 3. Rotation curved and velocity dispersion profiles for Sa galaxies, varying the concentration of the bulge relative to the disk components, and the inclination angle i . All the quantities are referred to a galaxy of $M = 10^{11}M_{\odot}$, and $R_e = 10$ kpc. The scaling factor is described into the text.

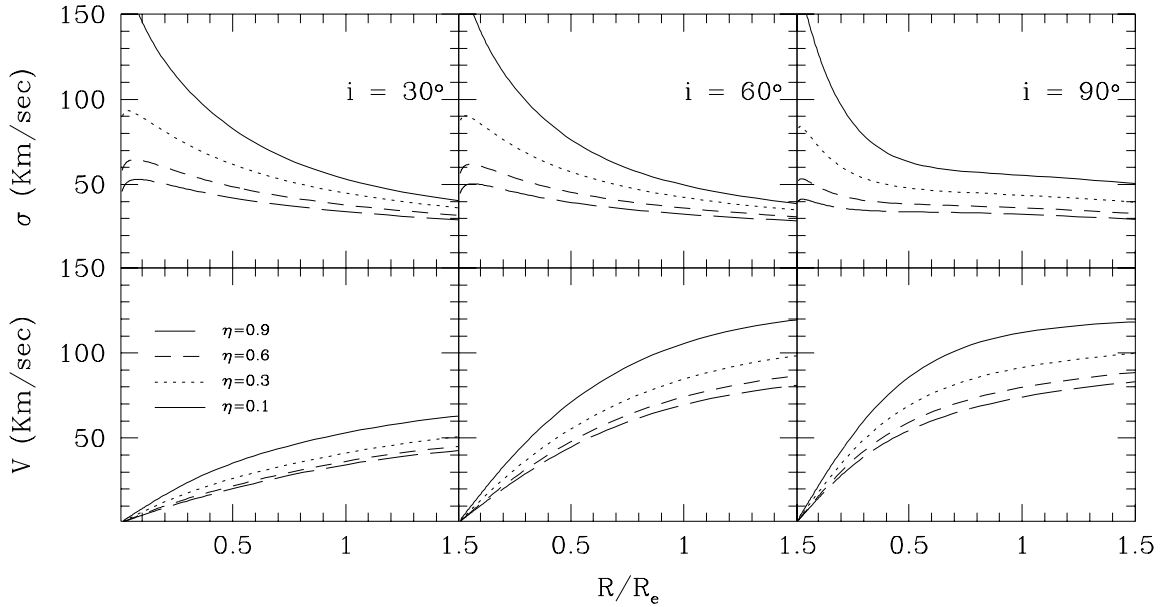


Fig. 4. Rotation curved and velocity dispersion profiles for Sab galaxies, varying the concentration of the bulge relative to the disk components, and the inclination angle i . All the quantities are referred to a galaxy of $M = 10^{11}M_{\odot}$, and $R_e = 10$ kpc. The scaling factor is described into the text.

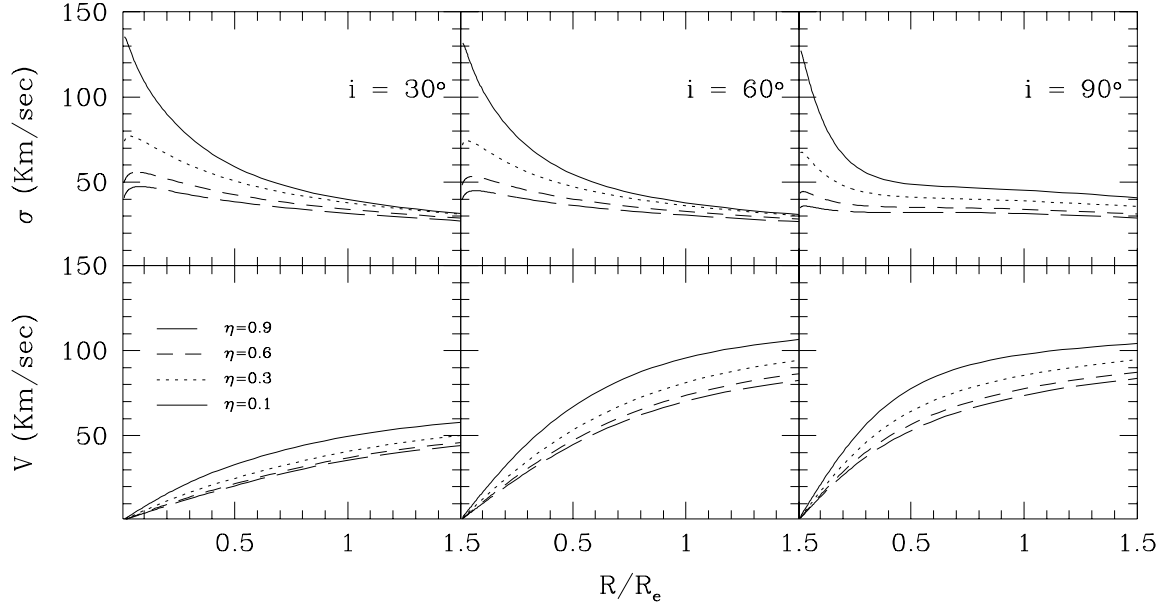


Fig. 5. Rotation curved and velocity dispersion profiles for Sb galaxies, varying the concentration of the bulge relative to the disk components, and the inclination angle i . All the quantities are referred to a galaxy of $M = 10^{11}M_{\odot}$, and $R_e = 10$ kpc. The scaling factor is described into the text.

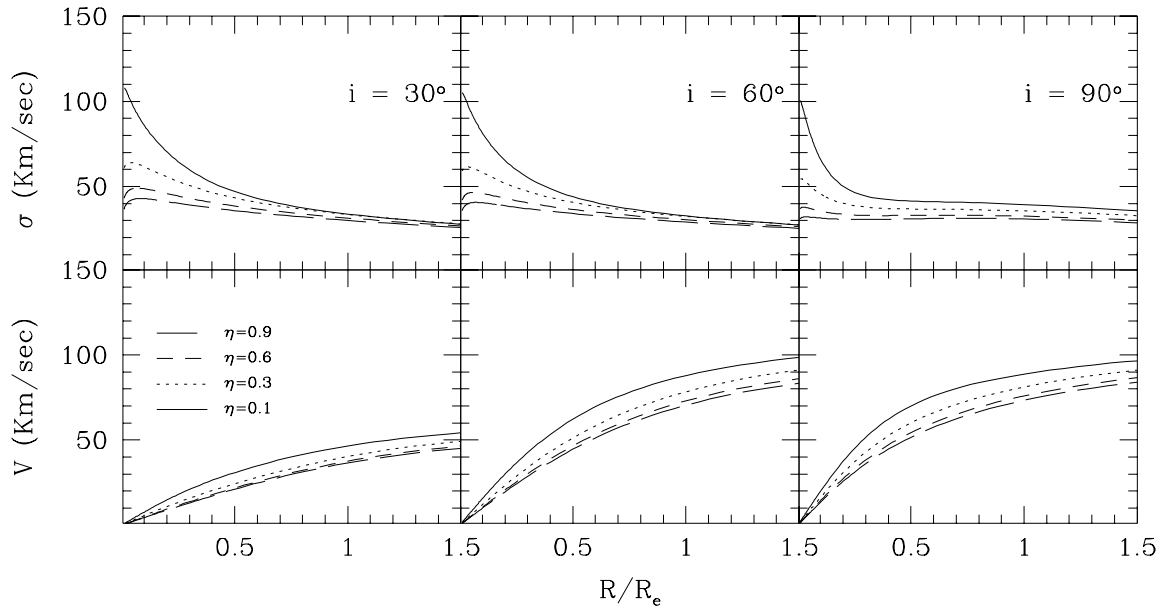


Fig. 6. Rotation curved and velocity dispersion profiles for Sbc galaxies, varying the concentration of the bulge relative to the disk components, and the inclination angle i . All the quantities are referred to a galaxy of $M = 10^{11}M_{\odot}$, and $R_e = 10$ kpc. The scaling factor is described into the text.

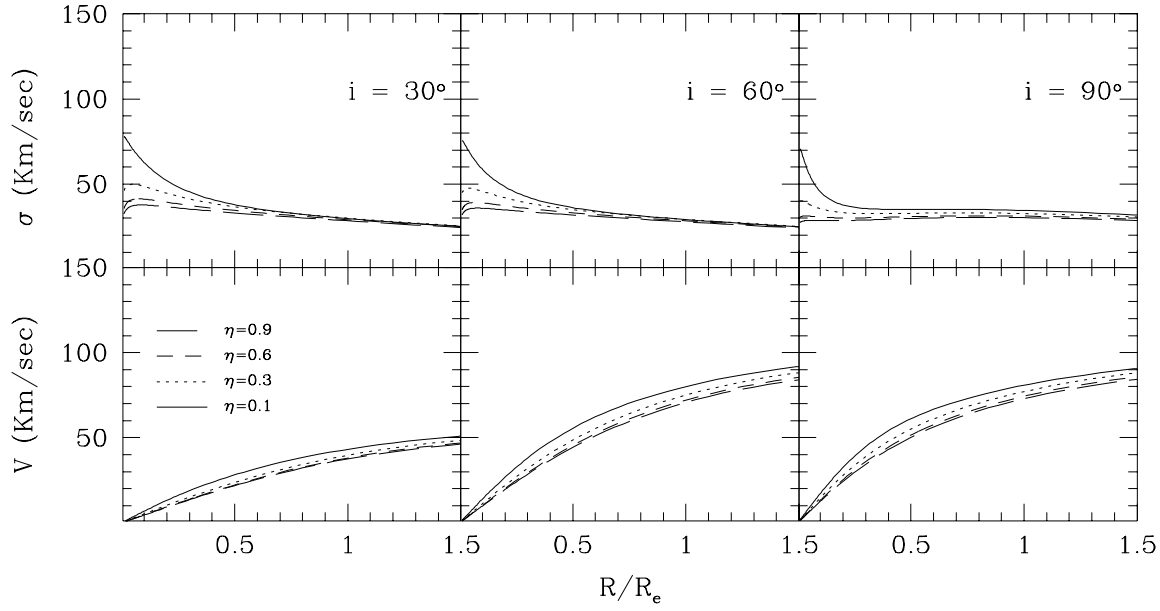


Fig. 7. Rotation curved and velocity dispersion profiles for Sc galaxies, varying the concentration of the bulge relative to the disk components, and the inclination angle i . All the quantities are referred to a galaxy of $M = 10^{11}M_{\odot}$, and $R_e = 10$ kpc. The scaling factor is described into the text.

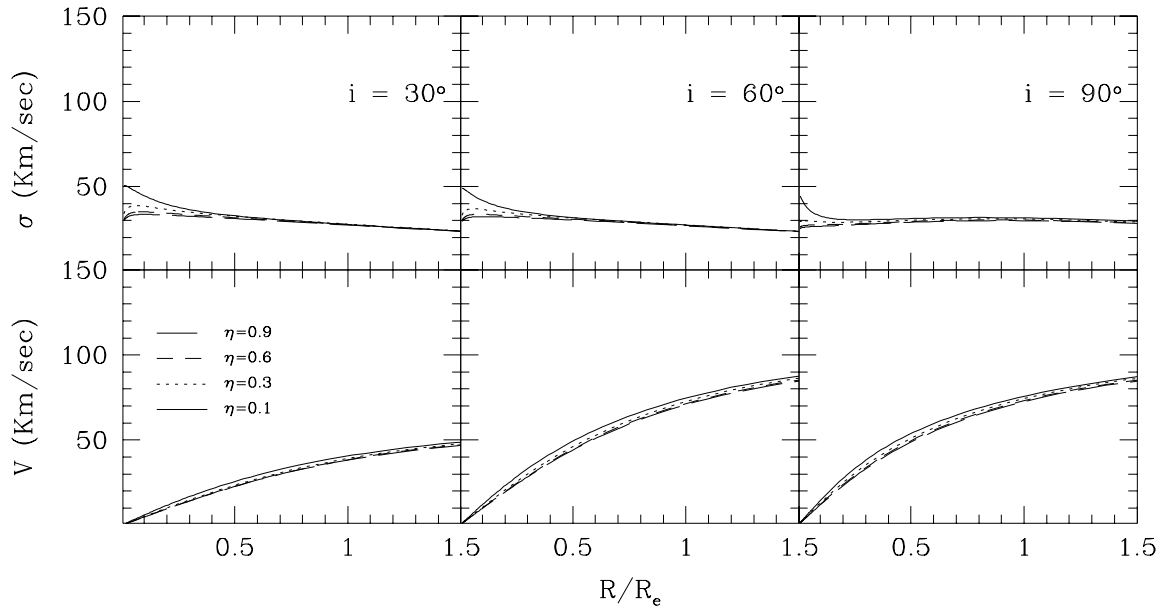


Fig. 8. Rotation curved and velocity dispersion profiles for Scd galaxies, varying the concentration of the bulge relative to the disk components, and the inclination angle i . All the quantities are referred to a galaxy of $M = 10^{11}M_{\odot}$, and $R_e = 10$ kpc. The scaling factor is described into the text.

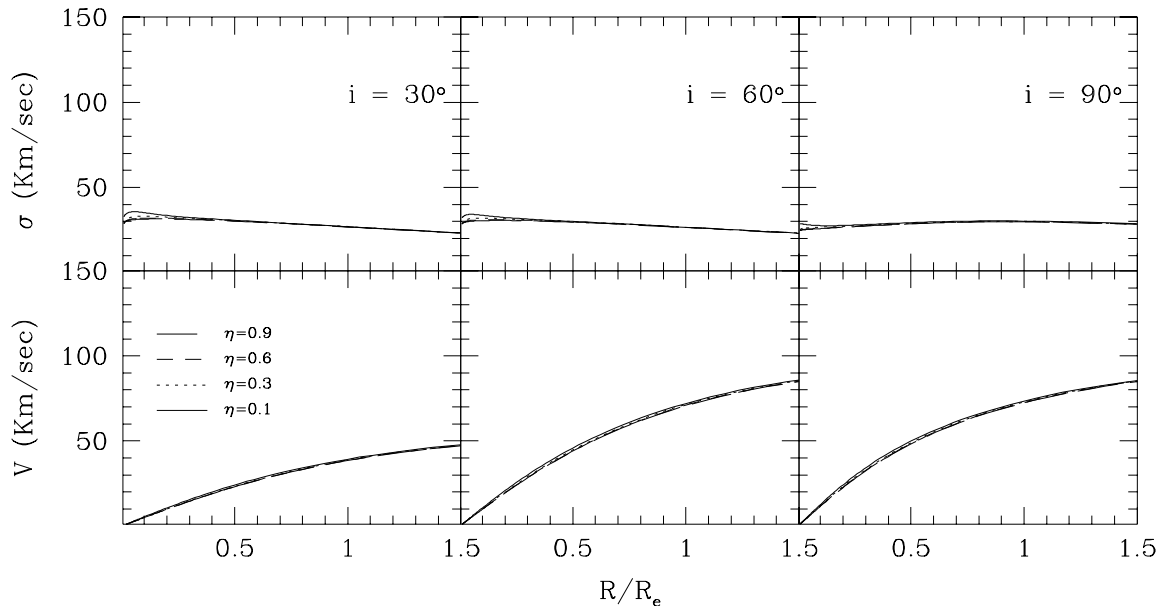


Fig. 9. Rotation curves and velocity dispersion profiles for Sd galaxies, varying the concentration of the bulge relative to the disk components, and the inclination angle i . All the quantities are referred to a galaxy of $M = 10^{11}M_{\odot}$, and $R_e = 10$ kpc. The scaling factor is described into the text.

the decomposition algorithms, that the photometric methods cannot be considered of general application (Seyfert & Scorza 1996).

A different approach may allow to deduce the ellipticity and anisotropy with a simultaneous fit of several rotation curves taken at different position angles or with offsets parallel to the major axis. This kind of data is available in the literature for an increasing number of galaxies and may be used to derive the anisotropy in their velocity distribution. The model presented here can support this kind of approach to estimate the amount of anisotropy present in an observed galaxy.

To this purpose, we shall discuss the effects of the two parameters (e, β) and their physical meaning. Under the hypothesis that the only ordered motion in the galaxy is the rotation around the z axis, the z component of the gravitation force can only be equilibrated by the z component of the velocity dispersion σ_{zz} , which is fixed once we have chosen a given distribution of matter, and *is not dependent from the anisotropy parameter β* .

Increasing the value of the anisotropy in the model, the *radial* component of the velocity dispersion increases, enhancing the importance of the asymmetric drift also. As β approaches unity, the value of σ_{RR} tends to infinity, and so the asymmetric drift. Following this trend, the asymmetric drift correction to the dynamical equation may overcome the gravitational term of equation (6), pulling the galaxy outward and destroying the dynamical equilibrium. As consequence, once fixed in a galaxy the axial ratio of the two components, not every values of β are allowed. The “physical” range of this parameter is restricted to $0 \leq \beta \leq \beta_{\max}(e)$, with $\beta_{\max}(e)$ derived by imposing:

$$\Delta V_{\text{asymdrift}}^2 < V_c^2 \quad (12)$$

in every point of the galaxy.

Since the circular velocity is not dependent from the anisotropy while the correction for asymmetric drift is related to it only by means of a scale factor, Eq. 12 can be rewritten as

$$f(e) \equiv \frac{\Delta V^2}{V_c^2}(\beta = 0) < 1 - \beta \quad (13)$$

so that the dependence from the β parameter is easy to handle.

The $f(e)$ can be computed analytically in the limit case of homogeneous spheroids only; the result is shown in Fig. 10. In the realistic case, with two-components and peaked density profiles, $f(e)$ must be computed numerically. We estimated the limiting β_{\max} from a set of models with bulges of different ellipticities. The results are shown in

Fig. 10, showing that the homogeneous spheroids curve can be used as a starting point for the analysis of the realistic cases.

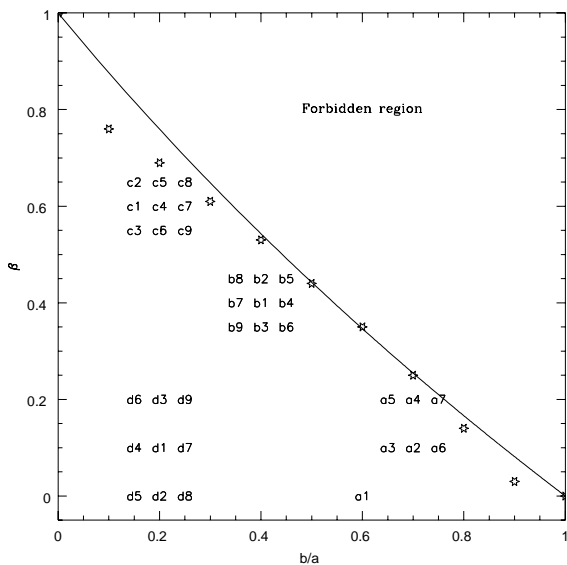


Fig. 10. The (β, e) plane. Below the solid line lies the physically allowed space of parameters, in the simple case of a single homogeneous spheroid. The maximum β allowed for different values of the axial ratio in the more realistic case of two-components galaxies are shown as starred points. The labels show the location of the models described in Tab. 2.

When a couple (e, β) has been found so that fit the major axis data in the permitted region of the $\beta - e$ space, the data along a different axis can be considered. In order to give a rough estimate of the diagnostic power of the model in determining the anisotropy parameter β , we choosed four models in different regions of the diagram, as shown in Fig. 10. They are labeled according to the codes defined in Tab. 2.

To test the possibility to distinguish different anisotropies from the observations, we compared different models assuming that the errors in observed quantities are $\Delta V = 20$ km/sec and $\Delta\sigma = 40$ Km/s and that rotation and σ curves are available along the apparent galaxy major axis and at an offset parallel to it but shifted by $0.5 R_e$. Models whose curves differs less than the above errors cannot be distinguished on observational basis. An example of this test is shown in Fig. 11, that is an anisotropic version of the S0 galaxy model with $\eta=0.5$ shown in Fig. 2. The representative points in the $\beta - e$ plane of this anisotropic model are labeled b in Fig. 10.

We can investigate the response of the projected kinematical curves of the models to small changes in the (β, e) values. We can distinguish three different cases:

1. **Almost spherical bulges** (Models a in Fig. 10). Under our assumption of homogeneous anisotropy, an almost spherical model ($b/a > 0.85$) does not allow solutions with significant anisotropy. The offset rotation curve is very sensitive to the β parameter changes, so that a $\Delta\beta$ of 0.1 generates a variation in velocity of 30% in the model. With $M = 10^{11} M_\odot$ and $R_e = 10$ kpc, this is equivalent to $\Delta V = 20$ km/sec.
2. **Strongly flattened bulges** (Models c and d in Fig 10). This is the opposite situation ($b/a < 0.4$). In this case, the diagnostic power of the model in determining anisotropy is limited. The offset curves give only poor additional information with respect to that obtained from the major axis data. However, in real galaxies this flattening is observed only in the late-type spirals, where the disc is preponderant with respect to the spheroidal component. As a consequence, the bulge gives a low contribution to the global kinematics.
3. **Intermediate models**(Models b in Fig. 10, also shown in Fig. 11). The higher efficiency of the models in distinguishing the anisotropy of a real galaxy from observations is found for galaxies with bulges having intermediate flatnesses ($0.4 \leq b/a \leq 0.85$). In this case, the physically allowed region in the space of parameters is large enough to justify a detailed search for the presence of anisotropy. In this situation, the offset rotation curves are pretty sensitive to the (β, e) values. The presence of an offset spectrum can half the uncertainties on the value of β derived

Table 2. Values of the anisotropy and flatness parameters for the models shown in Fig. 10

Model	b/a	β	Model	b/a	β
a1	0.6	0.0	b1	0.4	0.4
a2	0.7	0.1	b2	0.4	0.45
a3	0.65	0.1	b3	0.4	0.35
a4	0.7	0.2	b4	0.45	0.4
a5	0.65	0.2	b5	0.45	0.45
a6	0.75	0.1	b6	0.45	0.35
–	–	–	b7	0.35	0.4
–	–	–	b8	0.35	0.45
–	–	–	b9	0.35	0.35
c1	0.15	0.6	d1	0.2	0.1
c2	0.15	0.65	d2	0.2	0.0
c3	0.15	0.55	d3	0.2	0.2
c4	0.2	0.6	d4	0.2	0.1
c5	0.2	0.65	d5	0.2	0.0
c6	0.2	0.55	d6	0.2	0.2
c7	0.25	0.6	d7	0.2	0.1
c8	0.25	0.65	d8	0.2	0.0
c9	0.25	0.55	d9	0.2	0.2

from observations along the major axis. In such a case, starting from the observed V and σ curves at two different positions across the galaxy, a comparison with our model can give indication on the amount of anisotropy present.

6. Conclusions

We presented a self-consistent, two-components model of disc galaxy. We assumed that each component can be independently modeled by an ellipsoidal distribution of matter of constant axial ratio, and that the velocity distribution has an homogeneous anisotropy. Projected rotation- and velocity dispersion- profiles were produced changing the models parameters, to be compared with the observations.

In particular:

1. We produced a library of rotation curves and velocity dispersion profiles for different kind of galaxies along the morphological sequence. The sequence of models can be described by two parameters only: the relative weight and the concentration of the bulge with respect to the disc. Observed curves are generated changing the inclination angle of the galaxy. Such curves can be directly compared with observations of stellar kinematic by means of two scaling factors: one for the total mass of the galaxy, and another for the length scale.
2. The presence of anisotropy has been studied deriving the allowed region on the plane (β, e) (anisotropy-flattening) both analytically and by means of numerical computation. For each given value of the bulge axial ratio, a value β_{max} of the maximum allowed anisotropy has been established. In the extreme case of spherical systems, only isotropic distributions of velocities are allowed under our assumption of homogeneous anisotropy.
3. The models shows a strong diagnostic power in determining anisotropy in the bulges of the early-type disc galaxies when spectra outside of the apparent major axis are available. The best results are obtainable in the case of bulges of intermediate ($0.4 \leq b/a \leq 0.85$) flattening, close to the values observed in galaxies. In this case, an anisotropy change of 15% can give variations of 40-50% in the offset rotation curves, as shown in Fig. 11.

Acknowledgments

This work has been partially supported by the grant ‘‘Astrofisica e Fisica Cosmica’’ Fondi 40% of the Italian Ministry of University and Scientific and Technologic Research (MURST).

References

Bertola, F., Bettoni, D., Rusconi, L., Sedmak, G. 1984, AJ 89, 356

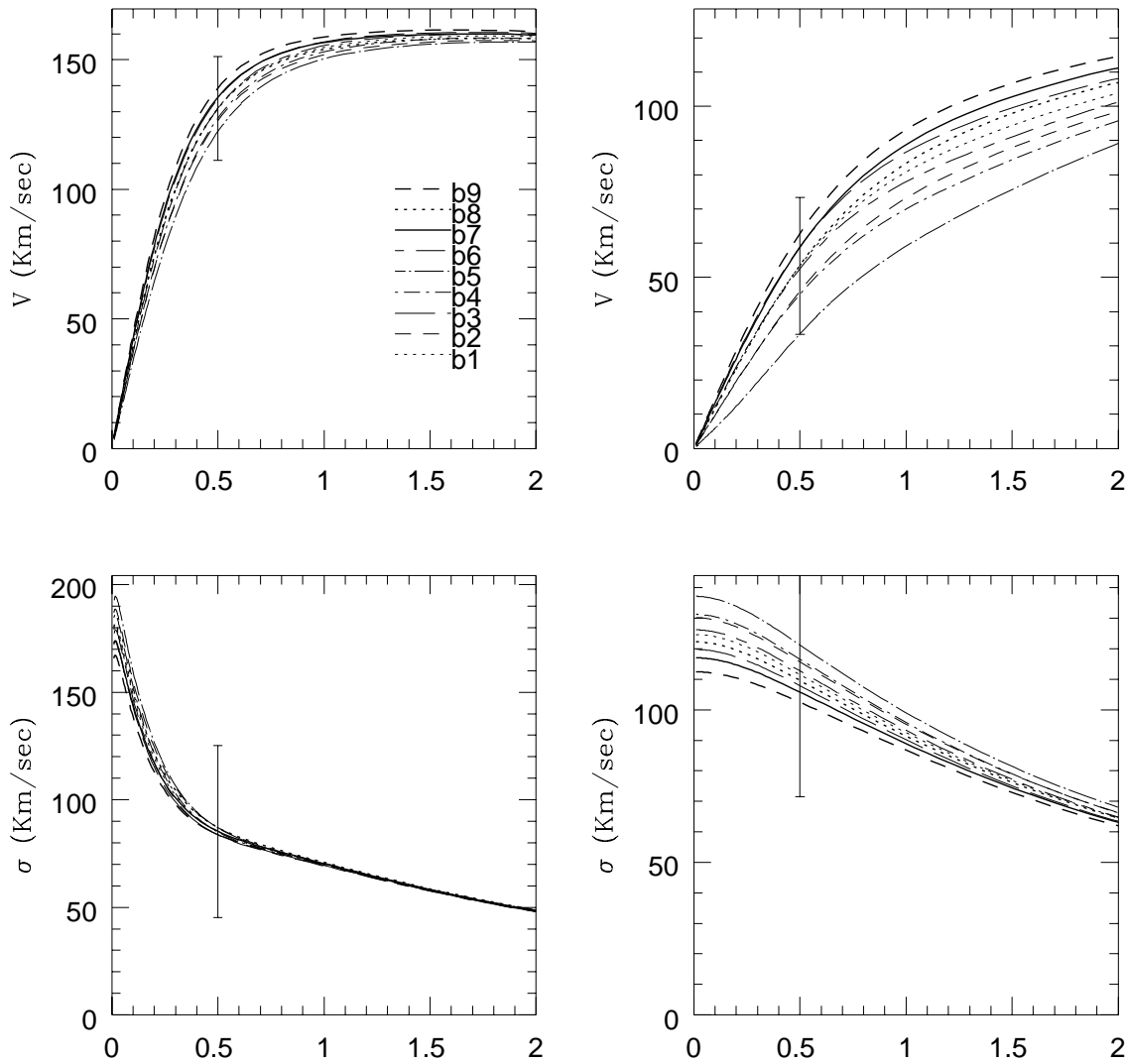


Fig. 11. An example of different kinematical curves along the major axis and along an offset parallel to the major axis shifted by $0.5 R_e$. The different curves correspond to an S0 galaxy with fixed ξ, η values but different (β, e) , chosen to produce similar V and σ curves along the major axis.

- Bertola, F., & Capaccioli, M., 1975 ApJ 200, 439
 Bertola, F., & Capaccioli, M., 1977 ApJ 211, 697
 Bertola, F., Vietri, M., Zeilinger, W.W., 1991, ApJ, 374, L13
 Binney, J. J. 1976, MNRAS. 177,19
 Binney, J. and De Vaucouleurs, G., 1991, MNRAS 194, 679
 Binney, J. J., Davies, R. L., Illingworth, G. 1990, ApJ 361,78
 Binney, J. & Tremaine, S., 1987, *Galactic Dynamics*, Princeton University Press
 Fillmore, J.A., Boroson, T.A., Dressler, A., 1986, ApJ, 302, 208
 Grosböl, P. J., 1985, A&AS 60, 261
 Kormendy, J., 1984, ApJ, 286, 116
 Kormendy, J. & Illingworth, G., 1982, ApJ 256, 460
 Kuijken, K. and Merrifield, M. R. 1993, MNRAS 264, 712
 Illingworth, G., & Schechter, P.L., 1982, ApJ, 256, 481

- Magrelli, G., Bettoni, D., Galletta, G. MNRAS 1992, 256, 500
 G. Monnet and F. Simien, 1977, A&A 56, 173
 Persic, M. & Salucci, P. 1995, ApJS 99, 501
 Pignatelli, E., PhD thesis
 Sandage, A., Freeman, K. and Stokes, N.R., 1970, ApJ 160, 831
 Sargent, W.L.W., Schechter, P.L., Boksenberg, A. and Shorridge, K. 1977, ApJ 212,326
 Simien, F. & De Vaucouleurs G., 1986, ApJ 302, 564
 Seifert, W., and Scorza, C., 1996, A&A 310, 75
 Stark, A. A. 1977, ApJ 213, 368
 Tonry, J.L. ApJ, 266,58
 Young,P.J., 1976, AJ, 81, 807
 van der Hulst, C.J., 1961 B.A.N., 509, 1
 Whitmore, B.C., Rubin, V.C., Ford, W.K., 1985, ApJ 287, 66
 Zeilinger W.W., Galletta, G., Madsen, C., 1990, MNRAS, 246, 324

A. The numerical computation

The equation of the model described above requires a 3-dimensional integration and a numerical derivation. Here we summarize the aspects of the numerical computation we think can be interesting to the reader.

A.1. A change of variable

We can rearrange Eqs. (8) with the following change of variable:

$$y^2 \equiv \frac{1}{\tau + 1}; \quad m'^2 \equiv \left(R^2 + \frac{z^2}{1 - e^2} \right) \quad (\text{A1})$$

obtaining:

$$\frac{\partial \Phi}{\partial R} = R G(R, z) \quad \frac{\partial \Phi}{\partial z} = \frac{z}{1 - e^2} G(R, z) \quad (\text{A2})$$

where

$$G(R, z) \equiv -4\pi G \int_0^1 \frac{\rho(m'^2)y^2}{\sqrt{1 - e^2}} dy \quad (\text{A3})$$

The basic advantage in the above formulation is that the integral in the definition of $G(R, z)$ is over the $(0, 1)$ interval, instead of $(0, \infty)$, thus making simpler the numerical integration. In addition, it makes obvious the relation between the two partial derivatives of the potential.

A.2. The surface brightness profile

A spheroidal distribution of light is characterized by a given axial ratio p and by a density profile of the form $\rho = \rho(R^2 + z^2/p^2)$. Its surface brightness profile $I(b)$ (where b is the projected radius) will, in general, depend from the axial ratio p , from the angle i between the z axis and the line of sight, and from the position angle Φ between the major axis and the axis used for the kinematic profile.

With this notation, the surface brightness is:

$$I(b) = \int_{-\infty}^{+\infty} \rho(R^2 + z^2/p^2) dl \quad (\text{A4})$$

Now we define $\hat{p}^2 \equiv p^2 \sin^2 i + \cos^2 i$: note that \hat{p}^2 is the apparent axial ratio of the galaxy as seen from the inclination i . Once that the relation between the coordinates systems (R, z) and (ℓ, b) has been written, Eq. A4 becomes

$$I(b) = \int_{-\infty}^{+\infty} \rho \left(\frac{\ell^2 \hat{p}^2}{p^2} + b^2 \frac{p^2 \cos^2 \Phi + \sin^2 \Phi}{p^2} \right) dl \quad (\text{A5})$$

With a change of the variable of integration we can then find the following, general result:

The surface brightness profile of a spheroidal luminosity density distribution with axial ratio p at an angle i of inclination and at a position angle Φ is equal to the value obtained in spherical distributions scaled for the flattening of the ellipsoidal distribution:

$$I_{\text{spheroidal}}(b) = \frac{p}{\hat{p}} I_{\text{spherical}} \left(\frac{\sqrt{\hat{p}^2 \cos^2 \Phi + \sin^2 \Phi}}{\hat{p}} b \right) \quad (\text{A6})$$

Since the surface brightness profile of the density profile of this model are analytical, we can thus derive the luminosity profile of each given model at any given position angle without having to compute it numerically, by a straightfor application of Eq. A6.